D-142 . Now in print. Vol 185, pp. 1016-43.

Combustion Science and Technology
Publication details, including instructions for authors and subscription information:
http://www.tandfonline.com/loi/gcst20

Flameholding in Converging and Turning Channels over Cavities with Slot Injection

Ben J. Colcord [a] , William A. Sirignano [a] & Feng Liu [a]
[a] Department of Mechanical and Aerospace Engineering, University of California, Irvine, CA
Accepted author version posted online: 12 Mar 2013.

To cite this article: Ben J. Colcord , William A. Sirignano & Feng Liu (2013): Flameholding in Converging and Turning Channels over Cavities with Slot Injection, Combustion Science and Technology, DOI:10.1080/00102202.2013.771075

To link to this article: http://dx.doi.org/10.1080/00102202.2013.771075

Flameholding in Converging and Turning Channels Over Cavities with Slot Injection

Ben J. Colcord, William A. Sirignano, and Feng Liu

Department of Mechanical and Aerospace Engineering, University of California, Irvine, California, USA

Abstract

Deliberate continuation of the combustion in the turbine passages of a gas turbine engine has the potential to increase the efficiency and the specific thrust or power of current gas-turbine engines. This concept, known as a turbine-burner, has challenges with the injection, mixing, ignition, and burning of fuel within a short residence time in a turbine passage characterized by large multi-directional accelerations. One method of increasing the residence time is to inject the fuel into a cavity adjacent to the turbine passage, creating a low-speed zone for mixing and combustion. This concept is simulated numerically, with the turbine passage modeled as a converging, turning channel flow of high-temperature, vitiated air adjacent to a cavity. Constant-area and converging channels with both straight and curving centerlines are modeled. Two-dimensional, unsteady calculations are performed, examining the effects of channel convergence and curvature, and injection configurations. These direct simulations address flows with Reynolds number values up to 5000. Calculations show that higher aspect ratio cavities improve the fluid interaction between the channel flow and the cavity, and that the cavity dimensions are important for enhancing the mixing. Results show that converging channels improve the combustion efficiency.

KEYWORDS: Combustion; Cavity flow; Direct numerical simulation; Gas turbine engine; Hydrodynamic instability; Turbine burner.

NOMENCLATURE

a, b	Chemical rate exponents
A	Pre-exponential reaction constant
D	Cavity depth, m
E_a	Activation energy, J/kg
Fr	Froude number
g	Gravitational acceleration, m/s^2
L	Cavity length, m
$\dot{m}$	mass flow rate, kg/s
M	Mixedness
Ma	Mach number
Re	Reynolds number
R_u	Universal gas constant, J/kgK
t	Time, s
T	Temperature, K
U	Freestream velocity, m/s
V	Volume, m^3
y_m	Modified mass fraction of element m
Y_m	Mass fraction of species m

Greek Symbols

α	Mixedness normalizing variable
Γ	Circulation, m^2/s
η_c	Combustion efficiency
τ_r	Residence time, s
Φ	Rayleigh discriminant, rad^2/s^2
Φ	Equivalence ratio
$\dot{\omega}$	Chemical reaction rate, kg/m^3s
Ω	Angular velocity, rad/s

Subscripts

C	Carbon atom
F	Fuel
i	Inflow
m	Index for chemical species
N	Nitrogen atom
p	Perfectly-mixed
∞	Freestream condition

1. INTRODUCTION

Thermodynamic analyses by Sirignano and Liu Sirignano and Liu (1999) show that purposely adding heat in the turbine of a gas-turbine engine has the potential to reduce

the afterburner length and weight and/or reduce the specific fuel consumption compared with turbojets with afterburners. Compared with turbojets without afterburners, the turbine-burner has the potential to increase the specific thrust. In a similar analysis for ground-based gas-turbine engines, the turbine-burner shows an increase in both specific power and thermal efficiency. From these analyses it is concluded that, contrary to the historical view that it should be avoided, augmented burning in the turbine passages offers an opportunity to improve the performance of gas turbine engines. This concept is known as a turbine-burner. A comprehensive review of the current turbine burner research has been presented by Sirignano et al. Sirignano et al. (2012)

Liu and Sirignano Liu and Sirignano (2001) extended the concept of the turbine-burner to include not only continuous burning in the turbine but also configurations where the turbine stators double as combustors, effectively introducing discrete inter-stage turbine-burners. The continuous turbine-burner (CTB) and the inter-stage turbine-burner with M stages (M-ITB) were compared with conventional turbojet and turbofan engines in a thermodynamic analysis. Both the CTB and the M-ITB show significantly higher specific thrust with no or only small increases in the thrust specific fuel consumption. The turbine-burner engines also perform consistently well across a wide range of flight Mach numbers and compressor pressure ratios, whereas the performance of the conventional engine declines rapidly outside of its operational range. The performance gain of turbine-burner engines over conventional engines increases with increasing compressor pressure ratio, fan bypass ratio, and/or flight Mach number.

The turbine passages are characterized by transonic, unsteady flows with very large three-dimensional accelerations. Combined with the relatively short length of the turbine passages, transonic flow speeds mean that the mixing, ignition, and burning of the fuel is required in a very short residence time. Additionally, the incoming flow from the combustor is a mixture of burned and unburned gases with significant spatial variations in temperature, composition, and density, which causes further complications.

Acceleration in the streamwise direction through the turbine passages can reach the order of 10^5g but, because of the transverse density gradient, the actual value of the streamwise acceleration will vary substantially in the transverse direction. This variation in turn creates large transverse velocity gradients, or highly strained flows. Strained flows can enhance mixing and heat transfer because of increased interface areas but the variations in local velocity can also create variations in residence times for different flow paths. This can produce further flammability difficulties where the residence times are shorter. One method of increasing the residence time of the flow is to use a cavity to create a low-speed zone where fuel and any additional air can be injected so that it has sufficient time for mixing and combustion to occur.

A discussion of relevant experimental and numerical research on flow over cavities by Hsu et al. Hsu et al. (1995, 1998), Katta and Roquemore Katta and Roquemore (1998a,b), Mathur et al. Mathur et al. (2001), Davis and Bowersox Davis and Bowersox (1997b,a), Yu et al. Yu et al. (1998, 2001a,b, 2003), Kim et al. Kim et al. (2004), Rasmussen at

al. Rasmussen et al. (2005), and Puranam et al. Puranam et al. (2009) has been given by Sirignano et al. Sirignano et al. (2012)

Our work here focuses on the coupling between the cavity flow and the flow in the simulated turbine stator passage with flameholding as one major goal. This goal differs from most of the above-mentioned works which aim at flameholding in scramjets or in compact combustors external to a turbine stage. The turbine passages in a gas turbine engine are characterized by large accelerations both in the streamwise and transverse directions due to the convergence and turning of the turbine blades. Also, it is only desirable to add enough fuel in the cavity/ turbine-stator to burn some but not all of the vitiated air entering the passage; that is, we still have a temperature-limited situation. Furthermore, the best strategy for combustion in the turbine nozzle vane is to have it begin in the upstream portion where the Mach number is lower. Nevertheless, effects of turning and streamwise acceleration are important and are examined in our analysis.

We have a few previous works on this turbine burner. For example, Purunam et al. Puranam et al. (2009) performed experiments with propane injection into a cavity in a curved, converging channel. They found that there are three distinct regimes for combustion depending on the air mass flow rates. At low air flow rates, the combustion is confined to the shear layer downstream of the cavity. At high air flow rates, combustion occurred almost exclusively in the cavity. At moderate flow rates, the flame was not stable in the cavity and fluctuated between burning in the shear layer and in the cavity.

Puranam et al. Puranam et al. (2009), using same type of cavity/channel configuration to the kind studied here (but a different injection scheme), achieved experimentally the desired enthalpy increase for a turbine burner.

Flow acceleration has been considered in flows without cavities. Sirignano and Kim Sirignano and Kim (1997) derived similarity solutions for a laminar 2-D mixing layer for both reacting and non-reacting flows with axial acceleration. It was shown that the mixing layer remains very thin for accelerating flow, and that the peak temperature was found to decrease with downstream distance. These results imply that NO_x formation would be less than that which occurs in a flow without acceleration. A mixing and exothermic chemical reaction in the accelerating flow through the turbine passage offers, therefore, an opportunity for a major technological improvement in both performance and pollutant mitigation. The reduction in peak temperatures due to acceleration results in the promise of reduced pollutant formation and reduced heat transfer losses in other combustion applications as well.

Fang et al. Fang et al. (2001) extended that study to mixing layers with arbitrary pressure gradients by using a finite-difference method for the boundary layer equations. The influence of pressure gradients, initial temperature, initial pressure, initial velocity, and transport properties were studied. Mehring et al. Mehring et al. (2001) performed a numerical study on a reacting, turbulent, and accelerating mixing layer. Cai et al. Cai et al. (2001) developed a finite-volume method for solving the two-dimensional compressible,

Favre-averaged Navier-Stokes equations with chemical reactions using the Baldwin-Lomax turbulence model. Cheng et al. Cheng et al. (2007, 2008, 2009) showed that, for accelerating transonic mixing layers, the shear layer instability for accelerating flows had smaller fluctuation compared to non-accelerating flows.

The Kelvin-Helmholtz instability occurs in most cavity flows due to the velocity shear at the upstream lip. The turbine passages in a gas turbine engine are characterized by large accelerations both in the streamwise and transverse directions due to the convergence and turning of the turbine blades. In two-dimensional flows, turning channels introduce two new modes of instability, the Rayleigh-Taylor instability and the Rayleigh centrifugal instability. The Rayleigh-Taylor instability occurs when a force acts in the direction of a density gradient. This situation is unstable if the density decreases in the direction of the force. The Rayleigh centrifugal instability occurs due to the dynamical effects of rotation or of streamline curvature. A necessary and sufficient condition for centrifugal stability is that $\Phi \geq 0$ everywhere, where Φ is the Rayleigh discriminant defined by

$$\Phi(r) = \frac{1}{r^3}\frac{d}{dr}\left(r^2\omega\right)^2. \tag{1}$$

where ω is the angular velocity in the curved channel. A broader review of turbine-burners is *given* by Sirignano et al. Sirignano et al. (2012).

The current work models a simplified turbine burner as a converging, turning channel flow over a cavity. The various channel/cavity geometries and injection configurations

are displayed in Figure 1 and discussed in Section 2. The calculations are primarily two-dimensional so the injection ports represent slot injection in three-dimensional space.

Section 2 presents the numerical models used, Section 3 gives the results of the numerical calculations for reacting flows in straight channels (3.1), converging channels (3.2), turning channels (3.3), and turning and converging channels (3.4). Finally, Section 4 gives our conclusions.

2. NUMERICAL MODELING

All calculations are performed using OpenFOAM (http://www.openfoam.com), an open-source C++ package. The 'reactingFoam' solver is used with additional modifications. The compressible, unsteady Navier-Stokes equations are solved together with conservation equations for energy and species mass fraction. The differencing schemes used are second-order accurate in both space and time.

The combustion is described as a one-step overall chemical reaction:

$$C_7H_{16} + 11(O_2 + 3.76N_2) \longrightarrow 7CO_2 + 8H_2O + 41.36N_2 \tag{2}$$

and the chemical kinetics rate for the fuel is calculated from

$$\dot{\omega}_F = -A\rho^{a+b}Y_F^a Y_O^b e^{-E_a/R_uT}, \tag{3}$$

where the chemical rate constants $A = 1.2 \times 10^9 \left(\mathrm{kg/m^3}\right)^{1-a-b}/\mathrm{s}$, $a = 0.25$, $b = 1.5$, and $E_a = 1.255 \times 10^8 \mathrm{J/kg}$ have been obtained from Westbrook and Dryer Westbrook and Dryer (1981).

As our results will show for this situation where hot vitiated air allows ignition, a thin diffusion flame will promptly be formed. So, detailed oxidation kinetics are not necessary here.

All of the reacting results presented here have a main channel flow inlet temperature of 1000K. The channel fluid is a vitiated mixture of 50% air and 50% combustion products. The temperature of the injected gaseous fuel or additional air is 300K. The Reynolds number is based on the channel height and inlet flow properties. The channel height has been fixed at 5cm so that *Re* varies with the inlet velocity. The cavity dimensions are denoted by $xxx \times yyy$, where *xxx* and *yyy* are the length and depth of the cavity, respectively, as percentages of the channel height, so that the numbers give both the size and aspect ratio of the cavity. For example, 200×050 represents a cavity 10cm long and 2.5cm deep. The equivalence ratio Φ represents the percentage of fuel compared to the overall stoichiometric conditions. The channel and cavity walls are adiabatic. Slip is allowed on the channel wall opposite to the cavity side in order to save computational costs.

For two-dimensional, slot-injection calculations, when fuel is injected from the upstream wall of the cavity, the oxygen initially in the cavity is quickly burned and replaced with combustion products. Since the injected fuel acts as a sheet, air in the channel cannot flow around the fuel into the cavity, as it could with a three-dimensional jet injection. Instead, the air must diffuse through the fuel. This limits the locations where fuel and oxidizer can react, lowering the combustion efficiency. All computations include air injection into the cavity. Four different injection configurations have been considered, as shown in Figure 1. The reinforcing configuration reinforces the natural rotation created by the main channel flow by injecting cold fuel high on the upstream wall and cold air low in the downstream wall. Conversely, the disrupting configuration injects the fuel low and the air high, disrupting the natural rotation. The parallel injection configuration has both fuel and air injected from the upstream wall while the opposing injection configuration has both injection ports high in the cavity on opposite walls. In three of the configurations, the air injection is downstream of the fuel injection. There is no reason to inject air upstream because vitiated air flows in the channel. The injection centerlines are 20% of the height of the cavity from the top or bottom of the cavity, and the port dimension is 2.5mm.

One parameter used to quantify the performance of different configurations is the combustion efficiency η_C. The combustion efficiency is a measure of how much of the fuel is consumed as a percentage of the amount injected. This fraction varies with time, so it is integrated to give an overall efficiency:

$$\eta_C = \frac{\int_{t_0}^{t_0+T} \int \dot{\omega}_F dV dt}{\int_{t_0}^{t_0+T} \dot{m}_{F,i} dt}, \tag{4}$$

where $\dot{\omega}_F$ is the fuel reaction rate. This definition is used for combustion efficiency rather than the more-commonly used definition using the fuel mass flow in and out of the domain. Both are equivalent as $T \to \infty$. However, the current definition appears to converge to a stable solution more quickly than when considering only fuel at the boundaries. This is because the current definition implicitly accounts for the change in the amount of fuel stored in the computational domain during the calculation, which is often significant for cavity flows. Flows over cavities are highly unsteady and oscillations can persist in the time integral of Eq. 4 for a prohibitively long time for numerical calculations. Where possible, the time evolution of Eq. 4 is presented rather than a single value for the combustion efficiency. The reader is then aware of any oscillations that may still be occurring in the value. Where a single representative value is given, it is the final time-averaged value at the termination of the calculation.

The overall combustion efficiency is influenced by the amount of mixing between the fuel and air, since fuel and oxidizer must mix before they can burn. Here, we define a mixedness parameter M locally as:

$$M = 1 + \frac{(y_C - y_{C,p})(y_N - y_{N,p})}{\alpha^2}, \tag{5}$$

where y_m is a modified mass fraction of element m that considers only carbon and nitrogen atoms:

$$y_m = \frac{Y_m}{Y_C + Y_N}. \tag{6}$$

The perfectly-mixed modified mass fraction, $y_{m,p}$, is calculated from the mass flow rates of air and fuel injected into the cavity. A normalizing variable α is used to enforce a mixedness of zero if completely unmixed for either Y_N or Y_C approaching zero. It is given by:

$$\alpha = \begin{cases} y_{C,p}, & (y_C - y_{C,p}) < 0 \\ y_{N,p}, & (y_C - y_{C,p}) > 0 \end{cases} \tag{7}$$

With complete mixing, a uniform mixture would result yielding a mixedness parameter of unity value.

A grid-dependence study was performed for a 200×050 cavity with disrupting injection configuration and an equivalence ratio of 0.25. The Reynolds number based on the inlet conditions is $Re = 2000$. Instantaneous profiles are shown in Figure 2 for two vertical slices; one at the center of the cavity and another at the exit of the channel. The legend shows the number of mesh points in each direction in relation to a coarse mesh. For example, the $X8$ mesh has twice the number of mesh points in each direction as the $X4$ mesh. This study shows that the $X10$ grid is sufficient for these calculations. A similar analysis showed that the $X20$ mesh is sufficient at $Re = 5000$.

The profiles in Figure 2 also illuminate important physical features of the flow. Figures 2(b) and 2(c) clearly show a diffusion-flame character and 2(d) shows that most of the mixing occurs in the shear layer. There is a sign-change in Figure 2(b), showing re-circulation in the cavity. The reaction rate at the channel exit is reduced by an order of magnitude from the center of the cavity but the diffusion-flame character remains.

The $X10$ grid used for the $Re = 2000$ calculations has 240×260 cells in the streamwise and normal directions, respectively. The non-uniform spacing gives a cell size of 0.0001 m normal to the bottom channel wall and in the center of the shear layer. Based on estimates of the shear layer thickness, this gives approximately 70 cells across the shear layer. This spacing is also approximately equal to the Kolmogorov length scale, though this constraint is not strictly necessary for two-dimensional transitional flows. The complete energy spectrum of turbulence has not formed; the three-dimensional microstructure has not developed; and therefore the Kolmogorov scale has no physical presence. The cell sizes in the streamwise direction in the cavity are more uniform and are $0.0003 - 0.0005$ m. The timestep is calculated using a CFL number of 0.5.

3. RESULTS

3.1. Reacting Flow in Non-Converging Channels

The time-averaged combustion efficiencies for the four configurations in a 200×050 and a 100×050 cavity at $Re = 2000$ are shown in Figure 3(a) and Figure 3(b), respectively. The efficiencies are plotted against time, beginning at 15s, the time at which the time-averaging

of the efficiencies was started. This startup time allows fuel and air to be injected into the cavity, to mix, ignite, and reach a state where the time-average of the efficiency does not depend on the starting time. Without this initial startup time, the cavity can still be filling with fuel, which gives an inaccurate value for the efficiency. Note that the 15s startup time represents close to 200 channel residence times, and the majority of that time is calculated using a coarser mesh to save computational time.

Figure 3(a) shows that, for the 200×050 cavity, the efficiencies for three of the four cases have reached relatively steady values after 0.25s, with only minor fluctuations in their values. The parallel injection configuration, however, shows a steady increase with time, indicating that a longer calculation time is required to get a converged combustion efficiency for this case. The parallel configuration is also the only one without significant high-frequency oscillations and appears to be steady or varying very slowly with time. This result likely occurs because it is the only configuration without any injection ports facing upstream so that relative velocities are reduced. The three other configurations do not vary significantly in their combustion efficiencies, but there is a reasonably clear ordering, with the reinforcing configuration having the highest efficiency followed by the opposing configuration and finally the disrupting.

Figure 3(b) gives the same information for the 100×050 cavity. For this shorter cavity, the injection configuration has a much greater effect on the combustion efficiencies. The parallel configuration again shows little sign of high frequency oscillations and is relatively

steady. However, with this cavity size the disrupting configuration is also relatively steady. These two configurations have the two lowest combustion efficiencies because of the lack of unsteady behavior promoting mixing. Again, the reinforcing and opposing configurations have the two highest efficiencies; although with this cavity size the opposing configuration has the higher efficiency.

The combustion efficiency is related directly to the fuel reaction rate, which is integrated over space and time to give an overall efficiency. The contours of the time-averaged reaction rate for the 200×050 cavity are shown in Figure 4. The disrupting configuration has a significantly reduced area of high reaction rate in the cavity, whereas the reinforcing injection has high reaction rates through most of the cavity. The average reaction rates in the main channel are similar for all configurations, except for the parallel injection.

Contour plots of the time-averaged mixedness are shown in Figure 5 for the 200×050 cavity. Instantaneous velocity vectors inside the cavities are also shown in Figure 6. With the exception of the parallel injection, the three other configurations are quite similar. The disrupting injection, with fuel injected near the cavity floor, has a relatively large region of low mixedness near the fuel injector, while the reinforcing and opposing configurations have only small regions of low mixedness near the fuel injector. The velocity vectors show a small vortex near the fuel injector for the reinforcing and opposing configurations that is not present with the disrupting configurations, which explains the low mixedness region in the disrupting configuration. The mixedness for these three cases is significantly higher

in the upstream half of the cavity because the magnitude of the velocity is much smaller here, giving the fuel and air more time to mix.

The effect of the injection configuration has a greater effect on the combustion efficiency at higher Reynolds numbers, as seen in Figure 7 for $Re = 5000$. Here, the disrupting and opposing configurations have significantly higher efficiencies than the parallel and reinforcing configurations. The air injection port is close to the top of the cavity, in the opposite direction to the channel flow, for the two cases with higher efficiencies. For the other two cases, the air injection port is near the bottom of the cavity where the velocity is low. The mixedness contours in Figure 8 show that the two cases with air injection near the cavity bottom have significantly larger areas in the cavity where mixedness is low, thus reducing the combustion efficiency. The temperature contours in Figure 9 also show that the low-temperature air jet has a greater effect in the cavity when injected near the bottom.

Table 1 shows the final values of the combustion efficiencies. The disrupting and reinforcing configurations show an increase in efficiency after doubling the length of the cavity, whereas the other two configurations show a decrease. It is therefore inconclusive as to which cavity size gives the best efficiency. Similarly, increasing the Reynolds number increases the combustion efficiency for two of the four cases.

A three-dimensional calculation was performed for the 200×050 cavity with disrupting injection, using the same two-dimensional boundary and initial conditions, and symmetry

conditions in the third dimension. Since computational resources are limited, fewer total mesh points were used in the x- and y-directions for the 3D mesh than were used in the 2D mesh. The mesh points in 3D were distributed so that they were more concentrated in regions where the 2D results suggested they were needed most; in the cavity and the downstream boundary layer. The near-wall mesh spacing for the downstream boundary layer was kept consistent with the 2D mesh, but fewer mesh points were used upstream of the cavity and in the upper half of the channel. Recall that slip is allowed on the upper channel wall so no boundary layer needs to be resolved. This redistribution of mesh points allows calculations with 40 mesh points in the z-direction. The 3D calculation showed an increase in combustion efficiency from 75.8% in the 2D case to 79.8% in the 3D case. This case was repeated in 2D using the exact mesh spacing as used in the 3D calculation so that any differences in the results come from the physical three-dimensional effects rather than any mesh effects. The two results are almost identical, indicating that three-dimensional effects are insignificant with two-dimensional boundary conditions at the given Reynolds number and the difference in the efficiencies are due to the coarseness of the 3D mesh. The remainder of the calculations will be two-dimensional.

3.2. Reacting Flow in Converging Channels

Only the disrupting and reinforcing injection configurations have been considered for the converging channel calculation. The opposing injection configuration is not considered because previous results indicate that the combustion efficiency falls between the disrupting and reinforcing configurations. This makes the opposing configuration less interesting than

the disrupting and reinforcing configurations. Three area convergence ratios of 2:1, 4:1, and 10:1 were considered. Here, the ratio is between the channel height at the inlet and the channel height at the exit. All of the channels converge linearly as shown later in Figure 11. The exit Mach number is less than 0.1 for all convergence ratios.

Figure 10 shows the combustion efficiencies of the disrupting injection cases. Here, it is clear that combustion efficiency increases with the convergence ratio. There is a significant improvement in efficiency from the non-converging channel to the 2:1 ratio converging channel, and the three converging channels all improve in efficiency as the convergence ratio increases. This occurs despite a decrease in the residence time of the channel, meaning that more fuel is burned in a shorter time.

Figure 11 shows the time-averaged reaction rate. This shows that the region of high reaction rates in the boundary layer thins as the convergence ratio increases. It is also evident that the region of high reaction rates in the cavity increases with the convergence ratio. In particular, the size of the region where the time-averaged reaction rate is 1.0 or higher increases noticeably as the convergence ratio increases. The 10:1 convergence ratio also exhibits a significantly larger region of high reaction rate than the lower convergence ratios. Note that the scale is logarithmic so the higher contour values are much more significant than the lower contours.

The reinforcing injection configuration also shows an increase in combustion efficiency with convergence ratio, as seen in Figure 12, but the trend is not as clear. Note that the converging channel cases were calculated over a longer time period since the time-integrated combustion efficiency was still varying. Even after doubling the calculation time the efficiency has still not completely stabilized. The non-converging channel and the 2:1 convergence ratio have the lowest efficiencies, both approximately 80%, with the 2:1 converging channel having a slightly lower final efficiency. The 4:1 and 10:1 converging channels both have final efficiencies of approximately 95%.

Figure 13 shows the time-averaged reaction rate for the case with reinforcing injection. The contours show similar trends to the disrupting injection, with a thinning of the high reaction rate region in the boundary layer offset by an increase in this region in the cavity. However, the second of these is not as clear as with the disrupting injection. It is clear, though, that compared with the disrupting injection configuration, the reaction rate in the lower half of the cavity is significantly higher. Figure 14 shows the velocity vectors for the 10:1 converging channel for the two injection configurations. Compared with the non-converging vectors in Figure 6, the disrupting injection shows an additional large vortex in the upstream portion of the cavity.

The inlet Mach number at $Re = 2000$ is approximately $Ma = 0.0082$, which gives an exit Mach number of approximately $Ma = 0.1$ with a 10:1 convergence ratio. To see the effects of compressibility, the inlet velocity was increased by a factor of 5 and the physical

domain was scaled down by the same factor to keep the same inlet Reynolds number. The reaction rate was increased by a factor of 25 to keep the same Damköhler number. These changes attempt to make the Mach number the only non-dimensional parameter that varies, yielding an exit value of about 0.5. Figure 15 shows the time-averaged combustion efficiencies for the low and high Mach number cases, respectively. The time scale for the high Mach number case has been rescaled to show the same number of residence times as the low Mach number case. The efficiencies have not converged completely, but the low Mach number case appears to have a slightly higher efficiency. Figure 16(a) and Figure 16(b) show the time-averaged reaction rates for the low and high Mach number cases, respectively. The contour levels are scaled so that the shading represents the same normalized value in each plot. While the high Mach number case has reaction occurring in a larger proportion of the cavity, the low Mach number case has higher peak reaction rate values. While we have kept the Reynolds number and Damköhler number constant based on upstream property values, the effects of compressibility at higher Mach numbers tend to decrease the residence time and the temperature. That is, the downstream velocity increases more and the downstream temperature decreases more for the higher Mach number case. This explains why the reaction rates are lower for the higher Mach number case. The normalized time-averaged velocity fields are almost identical for the two cases. Figure 16(c) and Figure 16(d) show the time-averaged Reynolds stresses for the two cases, again normalized by the highest value for each case. The high Mach number case has larger Reynolds stresses in the cavity. This result probably occurs because the same fractional change in velocity is associated with a larger fractional change in pressure and density

at higher Mach numbers. The greater fluctuations in pressure and density lead to greater fluctuations in the velocity. These greater fluctuations also explain the larger reaction area in the higher Mach number case in Figure 16(b).

3.3. Reacting Flow in Constant Area Turning Channels

The channel is turned through up to 90° and the centerline arc length of the channel is kept at 0.4m, the same as the straight channel length. At $Re = 2000$ with a 90° turning angle the centrifugal acceleration is $118\,\mathrm{m/s^2}$ or approximately 12g, giving a non-dimensional Froude number of $Fr = 2.13$, where

$$Fr = \frac{V}{\sqrt{aL}} = \sqrt{\frac{R}{L}}. \tag{8}$$

Instability can occur due to the dynamical effects of rotation or of streamline curvature. Drazin and Reid Drazin and Reid (2004) states that Rayleigh's circulation criterion is a necessary and sufficient condition for centrifugal stability and is given by Equation (1) That is, angular momentum cannot decrease in the positive radial direction.

Figure 17 shows the computed variation of the angular velocity squared for one channel cross-section just downstream of the cavity. If this quantity increases everywhere then it is centrifugally stable. Recall that slip is allowed on the channel wall opposite from the cavity. With the cavity on the inside of the channel, there is a small decrease away from the inside wall of the channel, close to the cavity. With the cavity on the outside, there is a significant decrease in this quantity near the outside of the channel, again close to the

cavity. While both cavity locations show a decrease in the Rayleigh discriminant, the case with the cavity on the outside has a more significant decrease and is expected to be more centrifugally unstable.

Figure 18(a) and Figure 18(b) show the time-averaged combustion efficiencies of turning channels with the cavity on the inside and on the outside, respectively. The same scale is used in both figures to highlight that the case with the cavity on the outside has a higher combustion efficiency for all injection configurations. The straight-channel results fall between the two curved-channel results shown here. The ranking of the injection configurations is not consistent for the three different geometric configurations. Clearly, the injection location is of secondary importance to the location of the cavity. Since the channel centerline arc length is fixed, the distance along the channel wall from the cavity to the exit is greater with the cavity on the outside. Coupled with the fact that the freestream velocity is lower on the outside, there is a significant increase in the residence time with the cavity on the outside. This increased residence time is likely the primary reason for the increased combustion efficiency seen in Figure 18(b).

The time-averaged mixedness contours and instantaneous cavity velocity vectors for the three injection configurations are shown in Figure 19–Figure 21. With the cavity on the outside of the channel, the centrifugal force acts to push high-density fluid into the cavity and to push low-density fluid away from it. Therefore, the unburned fuel and air tend to be forced to remain in the cavity while the burned products are forced out into the channel.

The mixedness contours for the cases with the cavity on the outside are qualitatively different from those with the cavity on the inside. Regardless of the injection configuration, with the cavity on the outside the upstream portion of the cavity has predominantly high mixedness values, whereas the case with the cavity on the inside has high mixedness values only close to the upstream cavity wall and the shear layer between the channel and the cavity. The average mixedness in the cavity is therefore greater with the cavity on the outside. Since this appears to be independent of the injection configuration, it is an effect of the centrifugal acceleration forcing the high-density unburned reactants to remain in the cavity in the case with the cavity on the outside.

Figure 22 shows the final time-averaged combustion efficiencies for all four injection configurations. Negative turning angles represent cases with the cavity on the inside of the channel curvature, while positive angles represent the cavity on the outside. Both 60° and 90° turning angles are considered for each location and for all four injection configurations. There is a clear improvement by having the cavity on the outside. As discussed above, this trend occurs because the case with the cavity on the outside has a longer residence time and because the centrifugal acceleration promotes greater mixing.

3.4. Reacting Flow in Converging and Turning Channels

A more realistic representation of an actual turbine passage is a channel that turns and converges, creating acceleration in both the axial and the transverse directions. Here,

we consider channels turning through 90° with a 10:1 convergence ratio for the disrupting and reinforcing injection configurations.

Figure 23 shows the comparison of the combustion efficiencies for all of the converging cases with disrupting injection. The straight channel gives the highest efficiency and the cavity on the outside gives the lowest, contrary to the non-converging results. Compared with the equivalent non-converging cases, the converging channels show an improvement in combustion efficiency for all configurations. This increase occurs because there is more mixing in the cavity due to a higher local Reynolds number. As described above, the channel on the outside has a longer residence time, resulting in a higher efficiency in non-converging channels. In converging channels, the residence time decreases for all cases, but has a greater effect on the case with the cavity on the outside because a larger fraction of the reaction occurs in the boundary layer.

The time-averaged reaction rate contours and instantaneous velocity vectors are shown in Figure 24. The reaction rate contours are similar but the case with the cavity on the inside has a thicker high-value region across the shear layer. Also, the velocity vectors show that when the cavity is on the outside, the higher-velocity channel flow enters the top portion of the cavity, effectively reducing the area of the low-speed zone in the cavity, causing a reduction in the amount of fuel burned in the cavity.

Figure 25 shows an identical trend in the combustion efficiencies for the cases with reinforcing injection as with disrupting injection. Again, convergence increases the combustion efficiency for all injection configurations, but more significantly when the channel is straight or the cavity is on the inside. The final combustion efficiency changes very little between the non-converging and converging cases when the cavity is on the outside. Figure 26 also shows similar results to Figure 24, with increased mixedness in the cavity with the cavity on the inside and the channel flow entering the cavity when on the outside.

The inlet Mach number was varied in the same way as in Section 3.2. Table 3 shows a decrease in combustion efficiency at higher Mach number for all of the channel geometries considered. As explained in Section 3.2, this is due to compressibility reducing the residence time and the temperature.

All of the combustion efficiencies are summarized in Table 2. Convergence appears to have the largest effect, improving the efficiency more than turning. Also, converging channels appear to have higher combustion efficiencies without channel curvature, whereas a non-converging channel has the highest efficiency when the cavity is on the outside.

The non-converging channel with the cavity on the inside performs poorly compared to other configurations. However, the same cavity location in a converging channel causes the combustion efficiency to increase by more than 20%. This increase with convergence when

the cavity is on the inside is due to two factors. Firstly, channel convergence increases the local Reynolds number and turbulent mixing regardless of the location of the curvature or cavity location. Secondly, when the cavity is on the inside, the higher-speed channel flow curves out from the cavity, essentially increasing the size of the low-speed mixing region.

4. CONCLUSIONS

We have addressed important aspects for cavity combustion relevant to mixing and burning in the turbine stators that have not been addressed previously: effects of converging channels; effects of turning channels; the effects of disrupting injection versus other types; the roles of Rayleigh-Taylor and Rayleigh-centrifugal instabilities in these cavity-channel coupled flows. Two-dimensional unsteady direct numerical simulation of the multicomponent, reacting Navier-Stokes system of equations have been performed with various air and fuel injection configurations and consideration of different cavity-channel configurations.

Useful combustion efficiency and mixedness parameters for this unsteady reacting flow have been formulated and calculated.

The injection locations of fuel and air can have significant impacts on the flowfield and on the combustion efficiency. The effect of injection location is greater for smaller cavities and higher Reynolds numbers. The parallel injection configuration, which was the only one that did not have an injection location on the downstream wall, was much less unstable than

the other three configurations. This indicates that the flow patterns near the downstream lip of the cavity are central to the overall stability of the flow.

Combustion efficiency increases as the convergence ratio increases for all injection configurations. Flow acceleration improves the combustion efficiency by improving the mixing. As inlet Mach number increases at constant Reynolds number and Damköhler number, the combustion efficiency decreases.

For turning channels, plots of the mean angular velocity show that the case with the cavity on the outside is more likely to be susceptible to the Rayleigh centrifugal instability.

The combustion efficiencies for the two-dimensional configurations have the same ranking order for both the disrupting slot-injection cases and the reinforcing slot-injection cases. From highest to lowest combustion efficiency:

1. Converging, non-turning
2. Converging, turning, cavity on inside
3. Converging, turning, cavity on outside
4. Non-converging, turning, cavity on outside
5. Non-converging, non-turning
6. Non-converging, turning, cavity on inside

This suggests that channel convergence improves the combustion efficiency regardless of channel curvature or injection configuration. For non-converging channels, the cavity on the outside is preferable and the cavity on the inside is the least desirable. This situation occurs because the channel residence time is longer with the cavity on the outside and because the centrifugal acceleration forces the higher density unreacted reactants to remain in the cavity and the low-density products to exit. For converging channels, the cavity on the outside becomes poor because the channel flow penetrates into the cavity, essentially reducing the size of the low-speed mixing region.

ACKNOWLEDGEMENTS

The authors wish to thank the U. S. Air Force Office of Scientific Research for supporting this research through Grant FA 9550-06-1-0194 with Dr. Julian Tishkoff as the Scientific Officer. Dr. W. Mel Roquemore and Dr. Joseph Zelina of the Air Force Research Laboratory are also thanked for their helpful advice.

REFERENCES

Cai, J., Icoz, O., Liu, F., and Sirignano, W.A., 2001. Ignition and flame studies for an accelerating transonic mixing layer in a curved duct flow. *AIAA Paper 01-0180.*

Cheng, F., Liu, F., and Sirignano, W.A., (2007). Nonpremixed combustion in an accelerating transonic flow undergoing transition. *AIAA Journal* **45**, pp. 2935–2946.

Cheng, F., Liu, F., and Sirignano, W.A., 2008. Nonpremixed combustion in an accelerating turning transonic flow undergoing transition. *AIAA Journal*, **46**, pp. 1204–1215.

Cheng, F., Liu, F., and Sirignano, W.A., 2009. Reacting mixing-layer computations in a simulated turbine-stator passage. *Journal of Propulsion and Power*, **25**, pp. 322–334.

Davis, D.L., and Bowersox, R.D.W. 1997a. Computational fluid dynamics analysis of cavity flame-holders for scramjets. *AIAA Paper 97-3270*.

Davis, D.L., and Bowersox, R.D.W., 1997b. Stirred reactor analysis of cavity flame-holders for scramjets. *AIAA Paper 97-3274*.

Drazin, P.G., and Reid, W.H., 2004. *Hydrodynamic Stability*. Cambridge, 2nd edition.

Fang, X., Liu, F., and Sirignano, W.A., 2001. Ignition and flame studies for an accelerating transonic mixing layer. *Journal of Propulsion and Power*, **17**, pp. 1058–1066.

Hsu, K.-Y., Goss, L.P., and Roquemore, W.M., 1998. Characteristics of a trapped-vortex combustor. *Journal of Propulsion and Power*, **14**, pp. 57–65.

Hsu, K.-Y., Goss, L.P., and Trump, D.D., 1995. Performance of a trapped-vortex combustor. *AIAA Paper 95-0810*.

Katta, V.R., and Roquemore, W.M., 1998. Numerical studies on trapped-vortex concepts for stable combustion. *Journal of Engineering for Gas Turbines and Power*, **120**, pp. 60–68.

Katta, V.R., and Roquemore, W.M., 1998b. Study on trapped-vortex combustor-effect of injection on flow dynamics. *Journal of Propulsion and Power*, **14**, pp. 273–281.

Kim, K.M., Baek, S.W., and Han, C.Y., 2004. Numerical study on supersonic combustion with cavity-based fuel injection. *International Journal of Heat and Mass Transfer*, **47**, pp. 271–286.

Liu, F., and Sirignano, W.A., 2001. Turbojet and Turbofan Engine Performance Increases through Turbine Burners. *Journal of Propulsion and Power*, **17**, pp. 695–705.

Mathur, T., Gruber, M., Jackson, K., Donbar, J., Donaldson, W., Jackson, T., and Billig, F., 2001. Supersonic combustion experiments with a cavity-based fuel injector. *Journal of Propulsion and Power*, **17**, pp. 1305–1312.

Mehring, C., Liu, F., and Sirignano, W.A., 2001. Ignition and flame studies for an accelerating transonic turbulent mixing layer. *AIAA Paper 01-0190*.

Puranam, S.V., Arici, J., Sarzi-Amade, N., Dunn-Rankin, d., and Sirignano, W.A., 2009. Turbulent combustion in a curving, contracting channel with a cavity stabilized flame. *Proceedings of the Combustion Institute*, **32**, pp. 2973–2981.

Rasmussen, C.C., Driscoll, J.F., Hsu, K.-Y., Donbar, J.M., Gruber, M.R., and Carter, C.D., 2005. Stability limits of cavity-stabilized flames in supersonic flow. *Proceedings of the Combustion Institute*, **30**, pp. 2825–2833.

Sirignano, W.A., Dunn-Rankin, D., Liu, F., Colcord, B.J., and Puranam, S.V., 2012. Turbine burners: Performance improvement and challenge of flameholding. *AIAA Journal*, **50**, pp. 1645–69.

Sirignano, W.A., and Kim, I., 1997. Diffusion flame in a two-dimensional, accelerating mixing layer. *Physics of Fluids*, **9**, pp. 2617–2630.

Sirignano, W.A., and Liu, F., 1999. Performance Increases for Gas-turbine Engines through Combustion Inside the Turbine. *Journal of Propulsion and Power*, **15**, pp. 111–118.

Westbrook, C.K., and Dryer, F.L., 1981. Simplified reaction mechanisms for the oxidation of hydrocarbon fuels in flames. *Combustion Science and Technology*, **27**, pp. 31–43.

Yu, K., Li, J.G., Chang, X.Y., Chen, L.H., and Sung, C.J., 2001a. Investigation of fuel injection and flame stabilization in liquid hydrocarbon-fueled supersonic combustors. *AIAA Paper 01-3608*.

Yu, K., Li, J.G., Chang, X.Y., Chen, L.H., and Sung, C.J., 2003. Fuel injection and flame stabilization in a liquid-kerosene-fueled supersonic combustors. *Journal of Propulsion and Power*, **19**, pp. 885–893.

Yu, K., Wilson, K.J., and Schadow, K.C., 2001b. Effect of flame-holding cavities on supersonic-combustion performance. *Journal of Propulsion and Power*, **17**, pp. 1287–1295.

Yu, K., Wilson, K.J., Smith, R.A., and Schadow, K.C., 1998. Experimental investigation on dual-purpose cavity in supersonic reacting flows. *AIAA Paper 98-0723*.

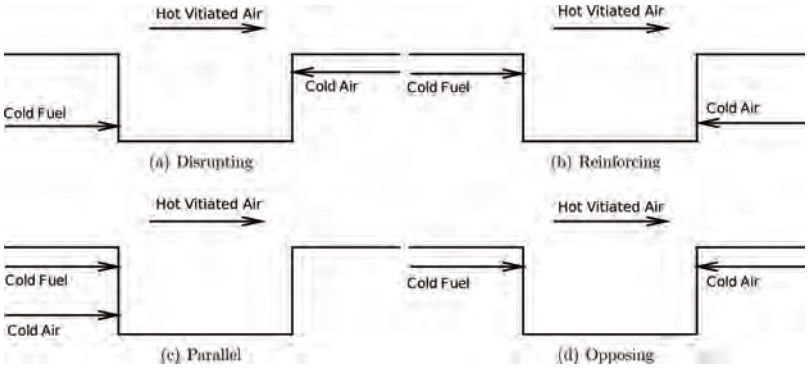

Figure 1: Injection configurations.

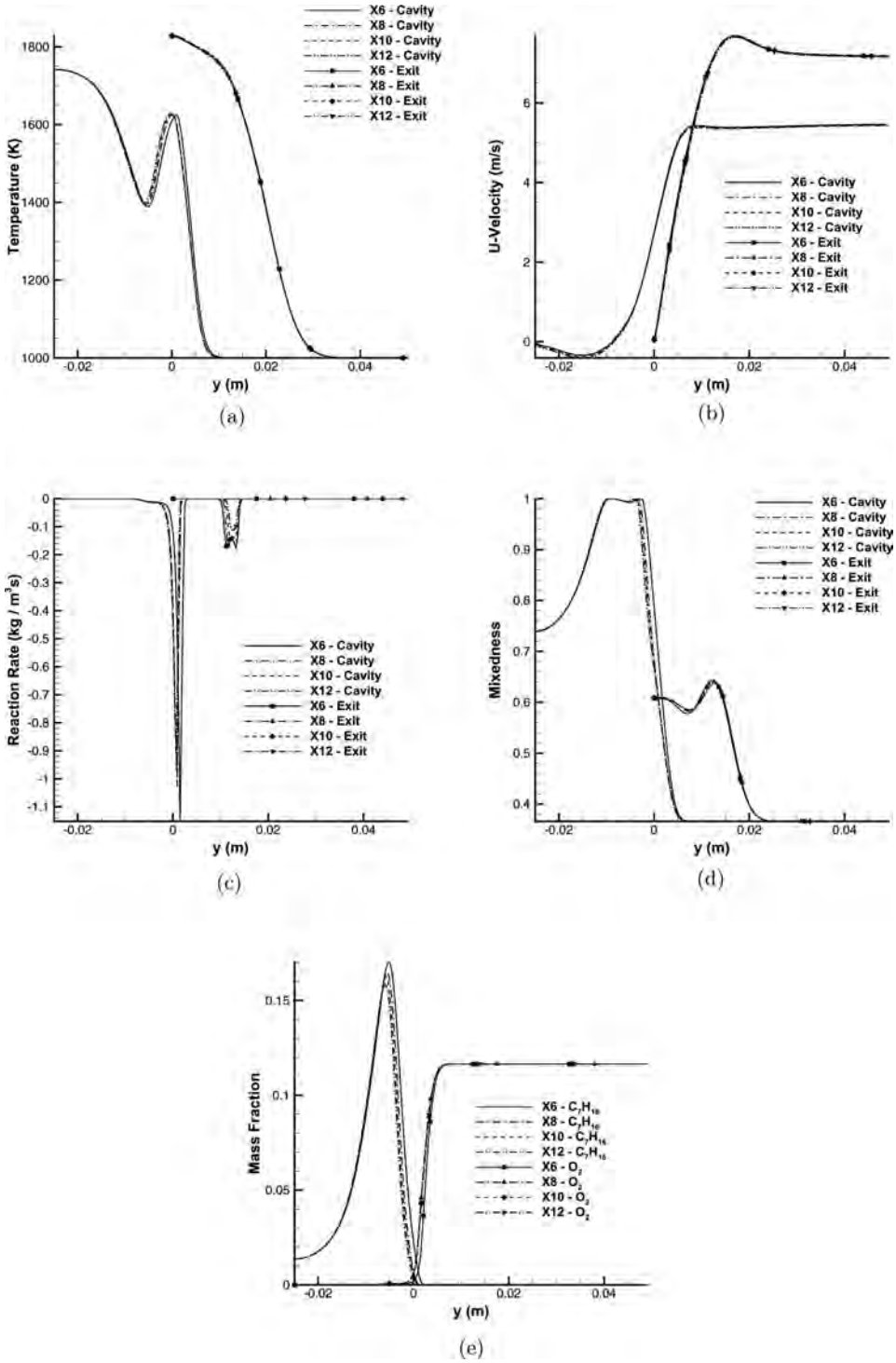

Figure 2: Instantaneous profiles at cavity center and channel exit.

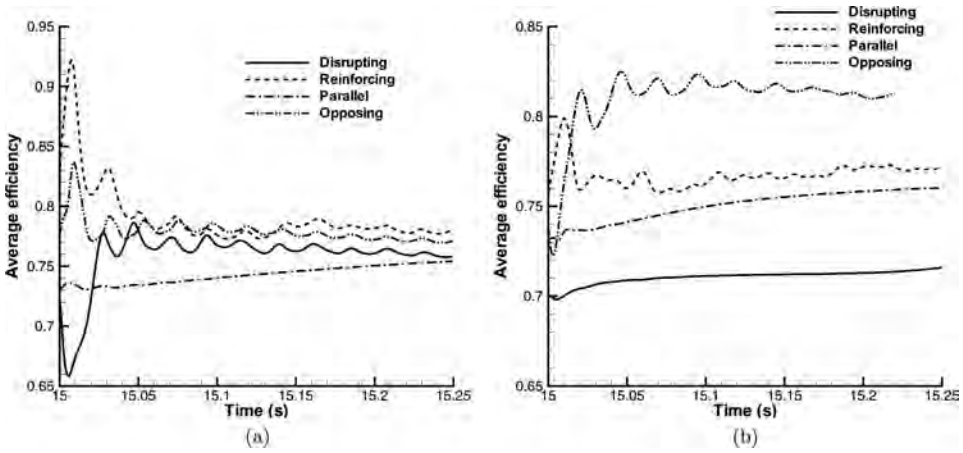

Figure 3: Effect of injection configuration on combustion efficiency in 2D cavities at $Re = 2000$.

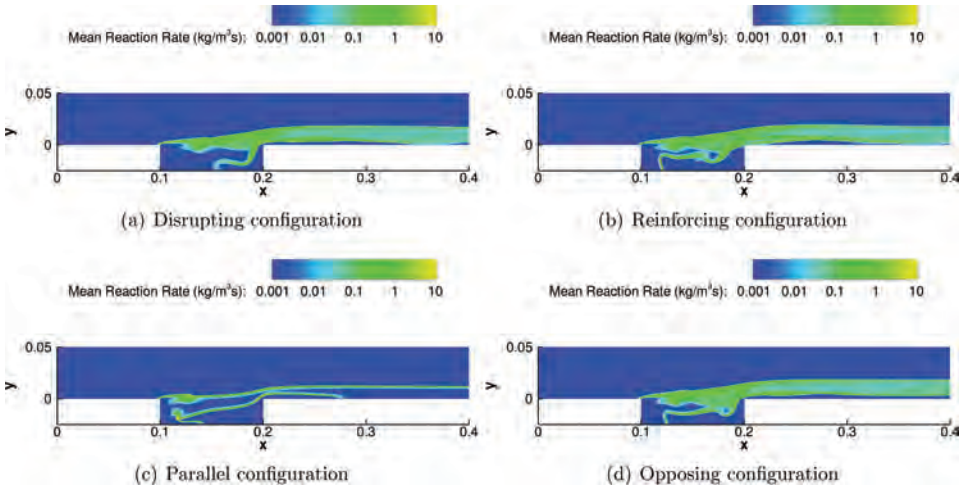

Figure 4: Reaction rates in 2D 200 × 050 cavities at $Re = 2000$.

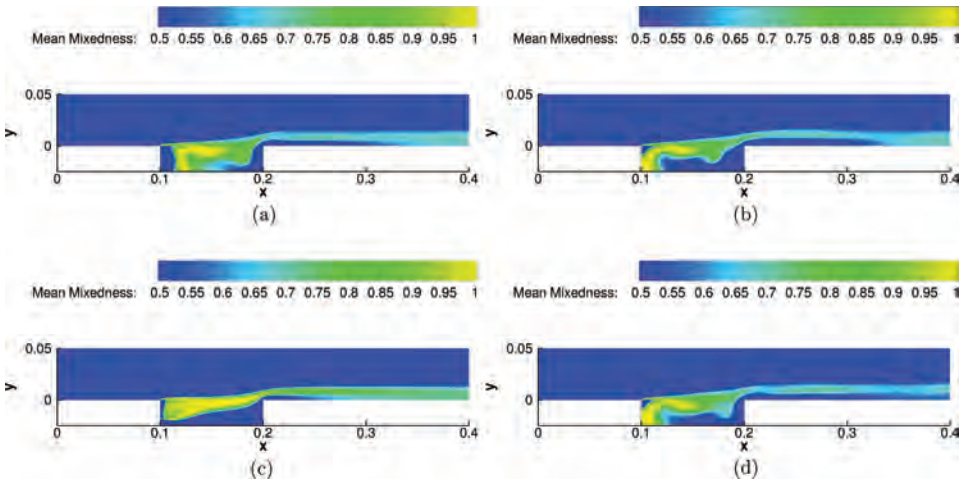

Figure 5: Time-averaged mixedness in 2D 200 × 050 cavities at $Re = 2000$.

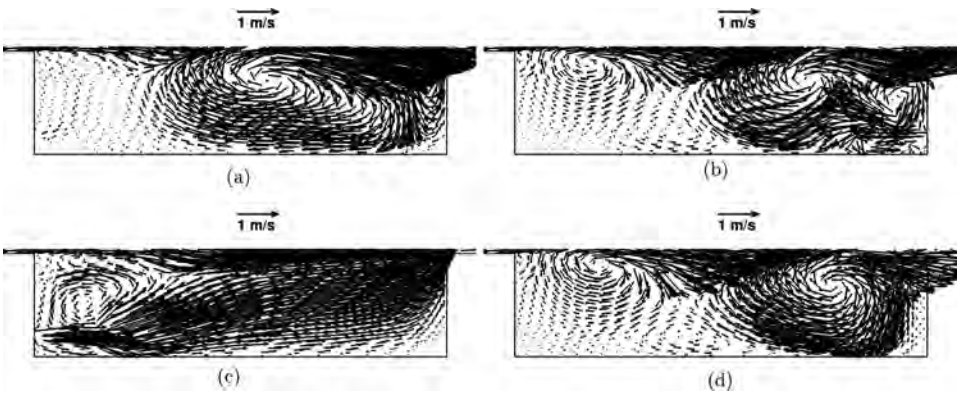

Figure 6: Instantaneous velocity vectors in 2D 200×050 cavities at $Re = 2000$.

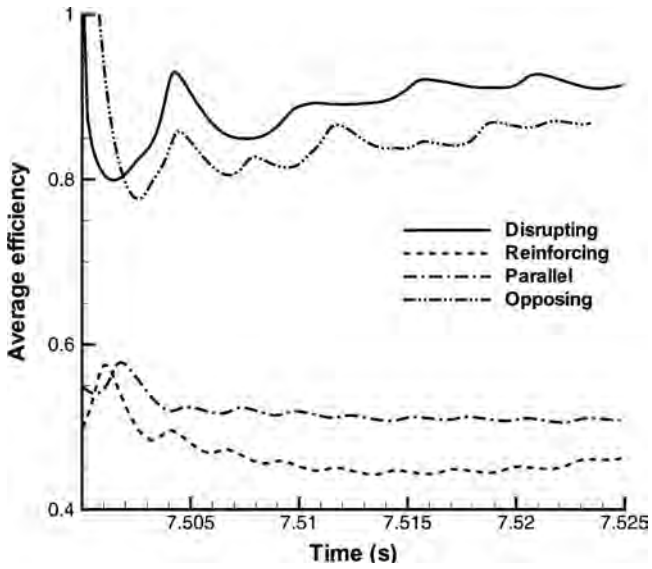

Figure 7: Effect of injection configuration on combustion efficiency in 2D 200×050 cavities at $Re = 5000$.

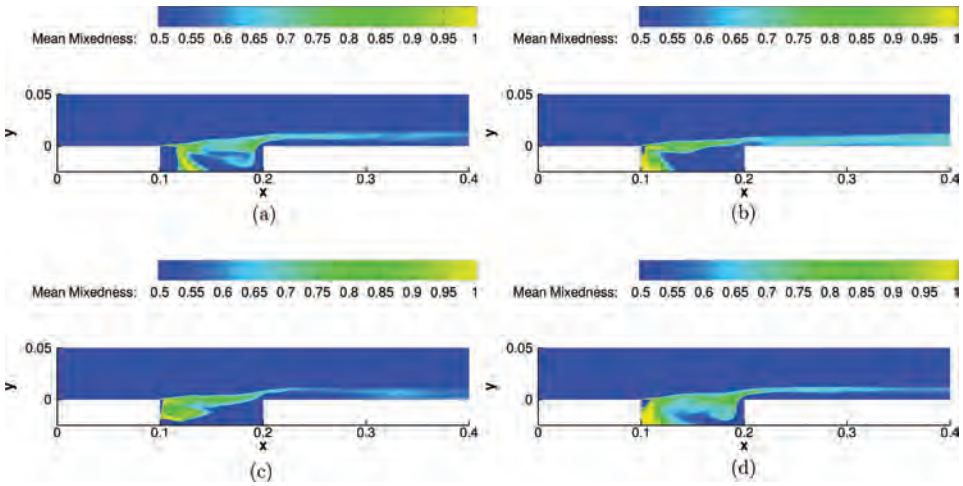

Figure 8: Time-averaged mixedness in 2D 200×050 cavities at $Re = 5000$.

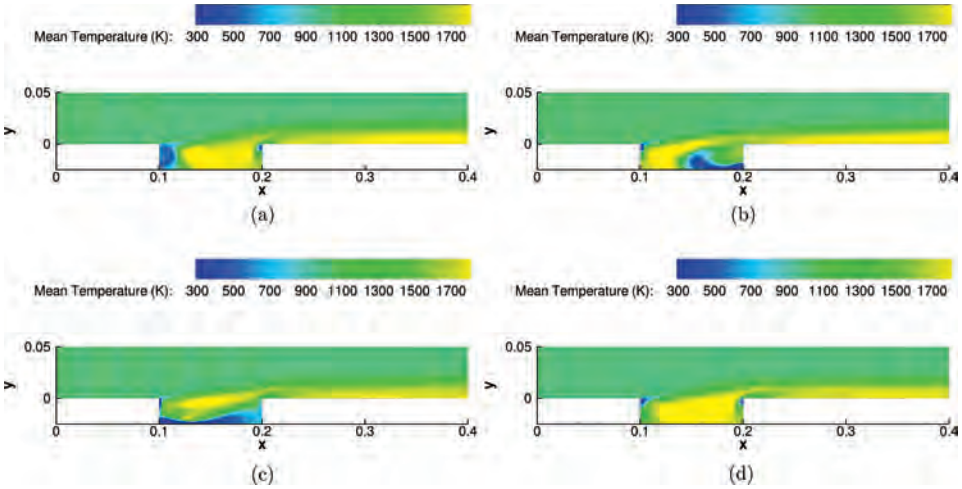

Figure 9: Time-averaged temperatures in 2D 200×050 cavities at $Re = 5000$.

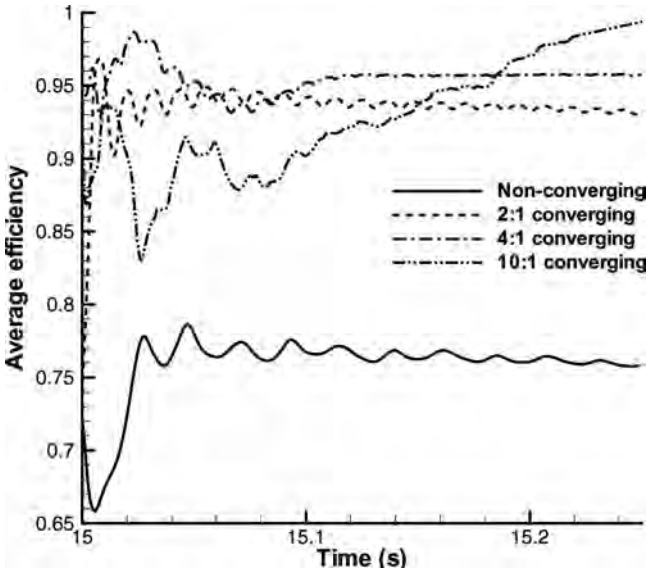

Figure 10: Combustion efficiencies for 2D non-converging and converging channels with a 200×50 cavity and disrupting injection at $Re = 2000$.

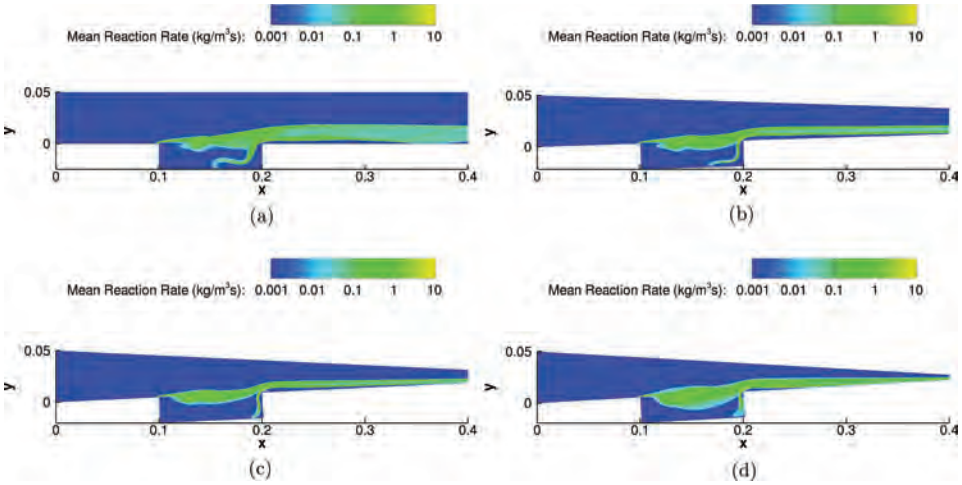

Figure 11: Time-averaged reaction rates in 2D 200×050 cavities at $Re = 2000$ with disrupting injection.

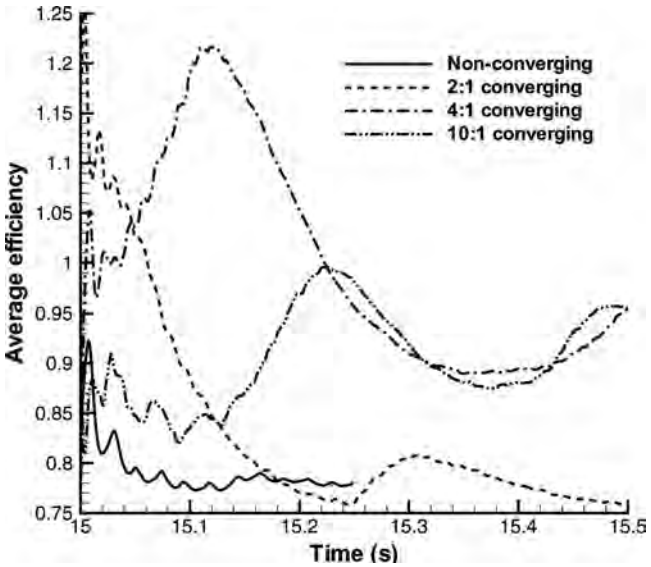

Figure 12: Combustion efficiencies for 2D non-converging and converging channels with a 200×50 cavity and reinforcing injection at $Re = 2000$.

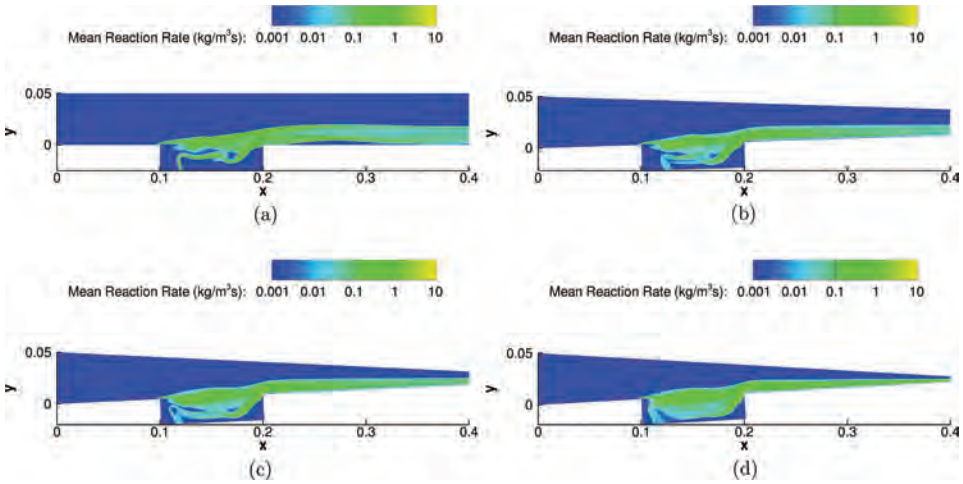

Figure 13: Time-averaged reaction rates in 2D 200×050 cavities at $Re = 2000$ with reinforcing injection.

Figure 14: Instantaneous velocity vectors in 2D 10:1 converging channels with 200×050 cavities at $Re = 2000$.

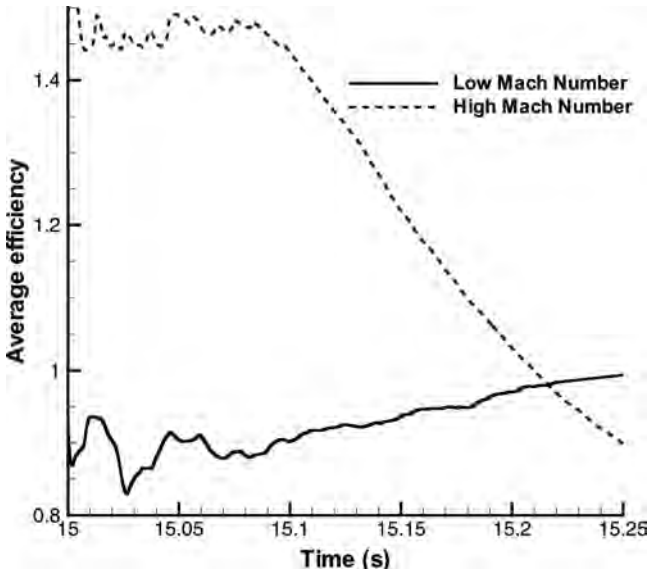

Figure 15: Combustion efficiencies for high- and low-Mach number 10:1 converging 2D channels with a 200×50 cavity and disrupting injection at $Re = 2000$.

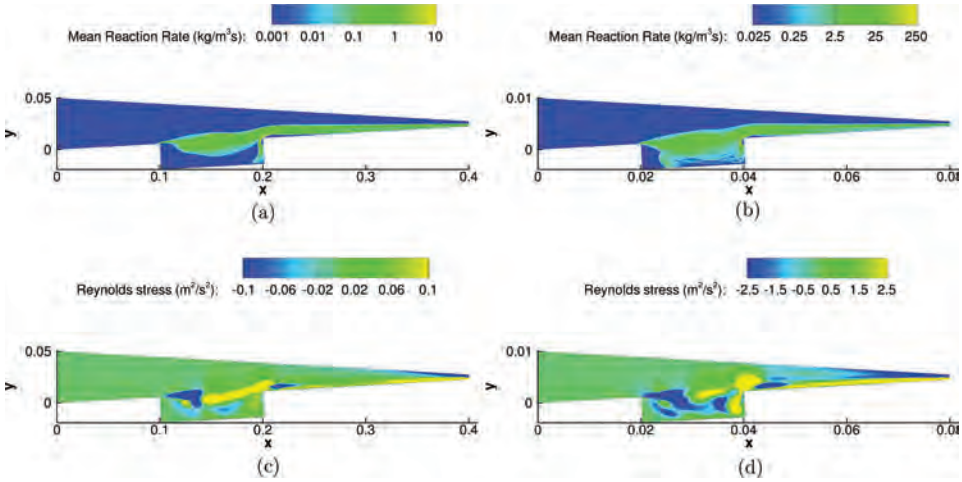

Figure 16: Time-averaged reaction rates and Reynolds stresses for high- and low-Mach number 10:1 converging 2D channels with a 200×50 cavity and disrupting injection at $Re = 2000$.

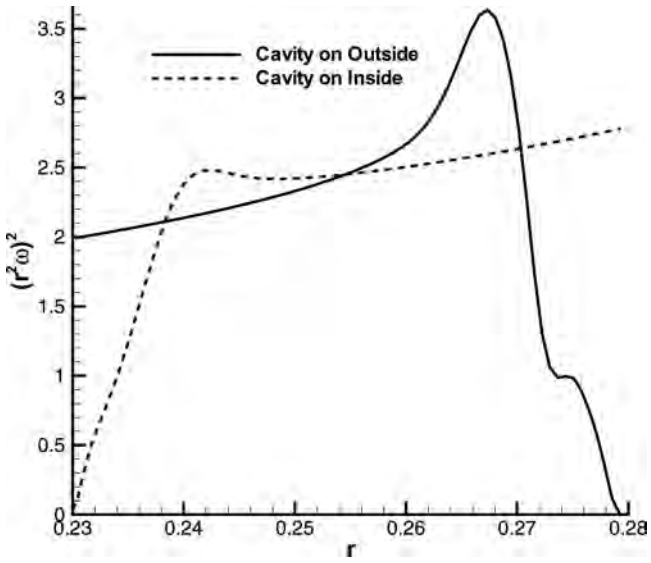

Figure 17: Rayleigh's circulation criterion for 2D, 90° turning channel with disrupting injection into a 200×050 cavity at $Re = 2000$.

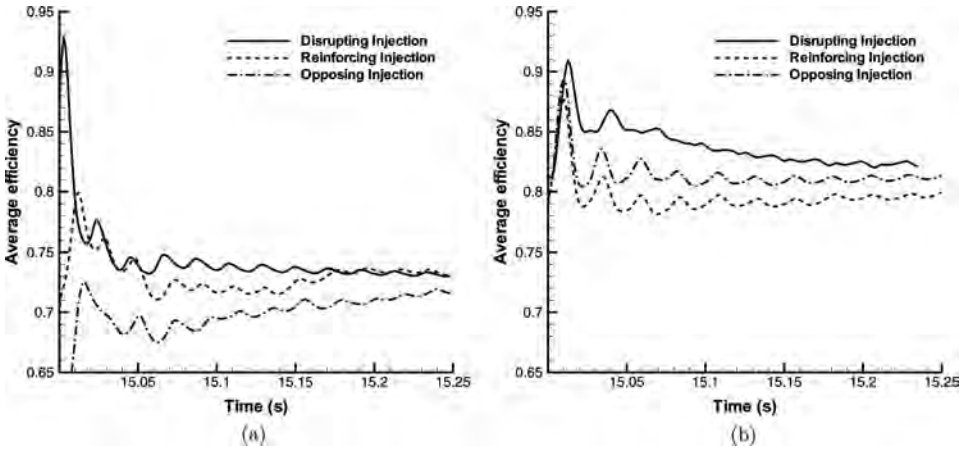

Figure 18: Combustion efficiencies in 2D, 90° turning channels with 200×050 cavities at $Re = 2000$.

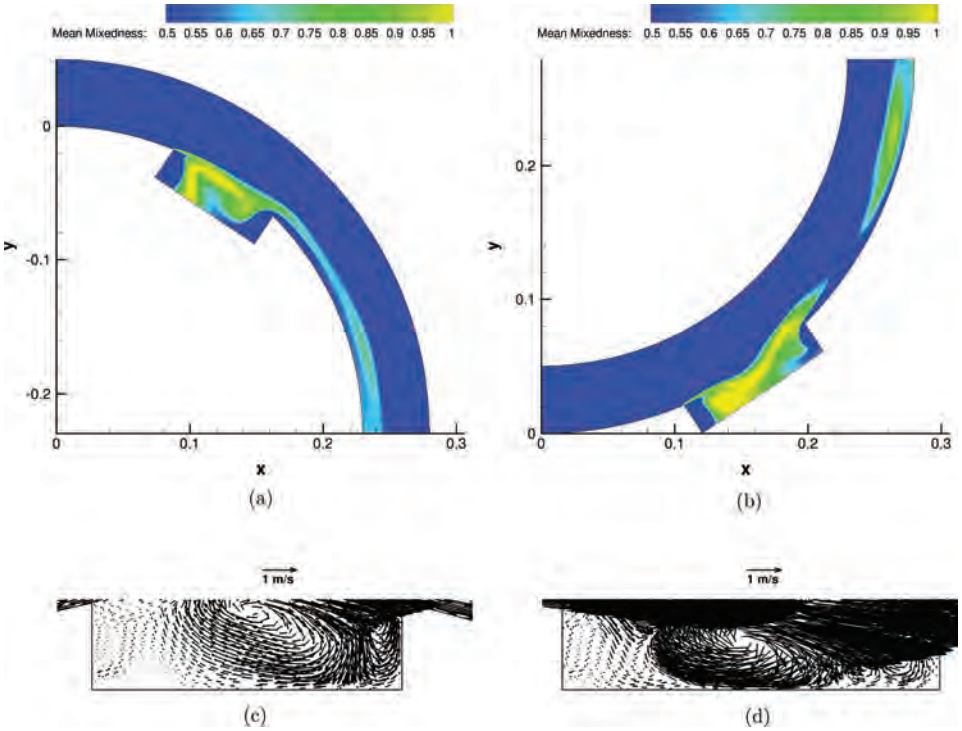

Figure 19: Time-averaged mixedness and instantaneous velocity vectors in $2D$, 90° turning channels with 200×050 cavities at $Re = 2000$ with disrupting injection.

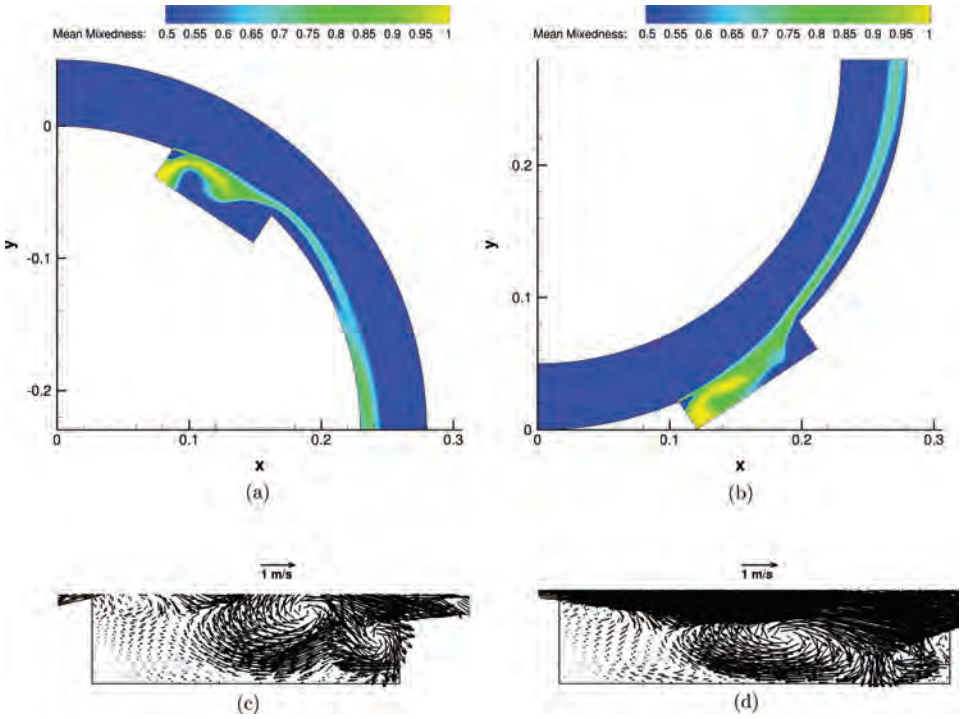

Figure 20: Time-averaged mixedness and instantaneous velocity vectors in 2D, 90° turning channels with 200 × 050 cavities at $Re = 2000$ with reinforcing injection.

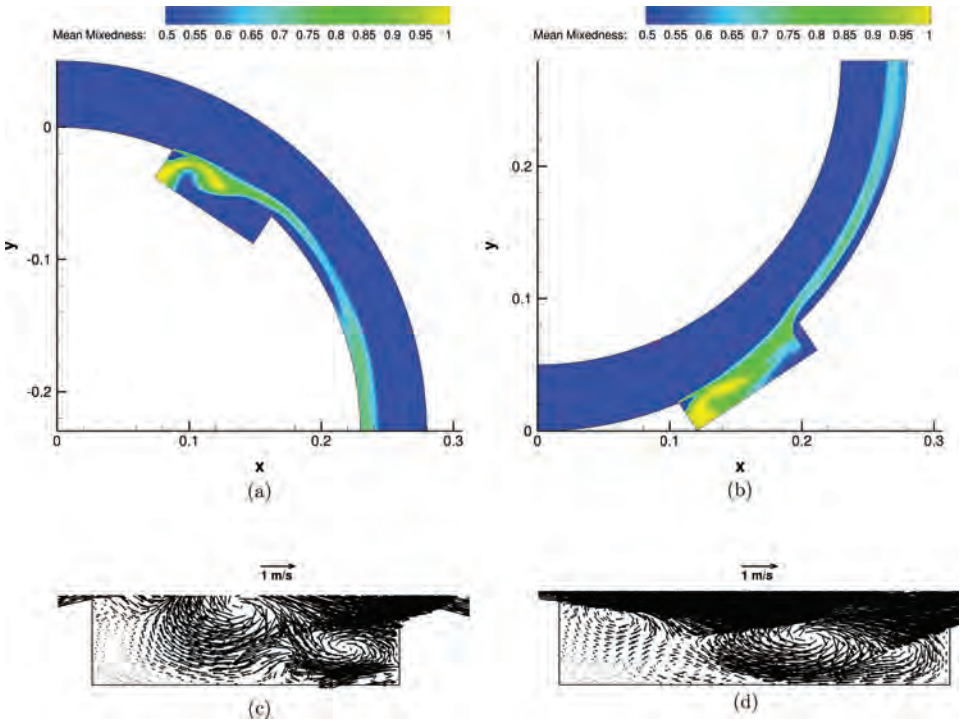

Figure 21: Time-averaged mixedness and instantaneous velocity vectors in 2D, 90° turning channels with 200×050 cavities at $Re = 2000$ with opposing injection.

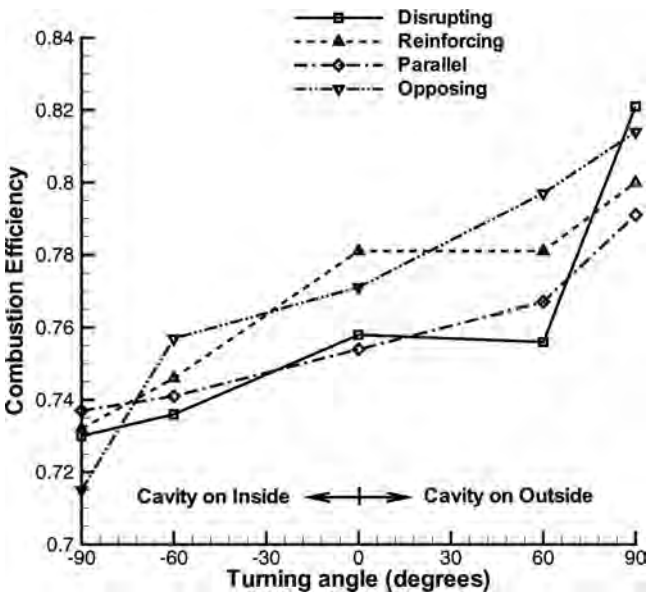

Figure 22: Combustion efficiencies in 2D, turning channels with 200×050 cavities at $Re = 2000$.

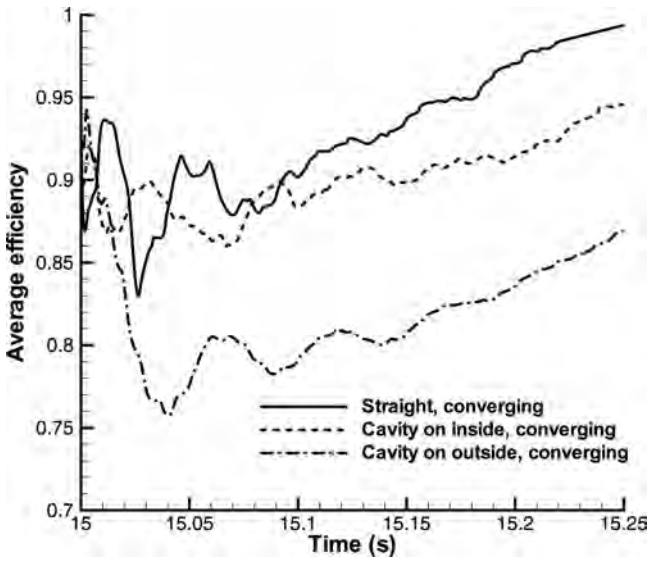

Figure 23: Combustion efficiencies for 2D, converging channels with 200×50 cavities and disrupting injection at $Re = 2000$.

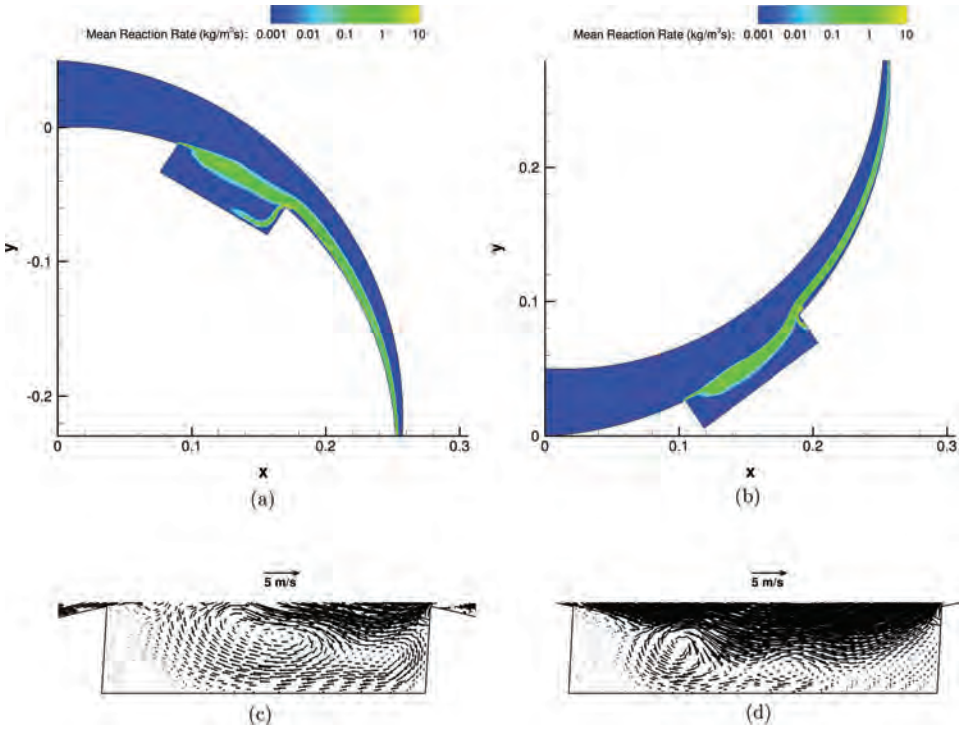

Figure 24: Time-averaged reaction rate and instantaneous velocity vectors in 2D, 90° turning, converging channels with 200 × 050 cavities at $Re = 2000$ with disrupting injection.

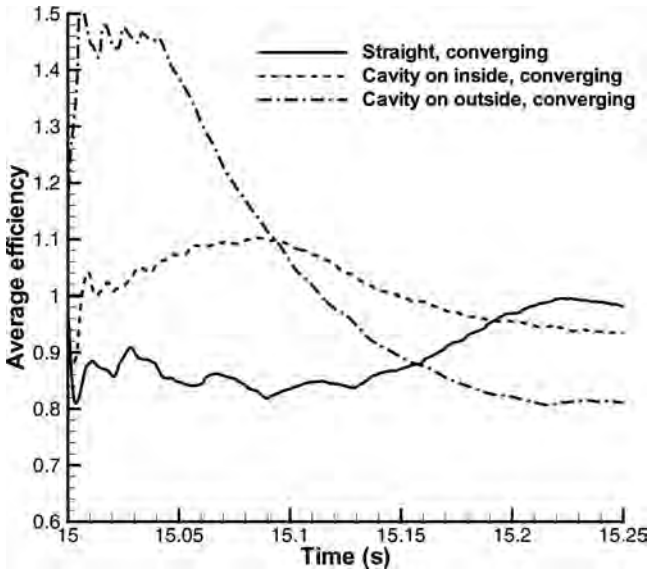

Figure 25: Combustion efficiencies for 2D, converging channels with 200×050 cavities and reinforcing injection at $Re = 2000$.

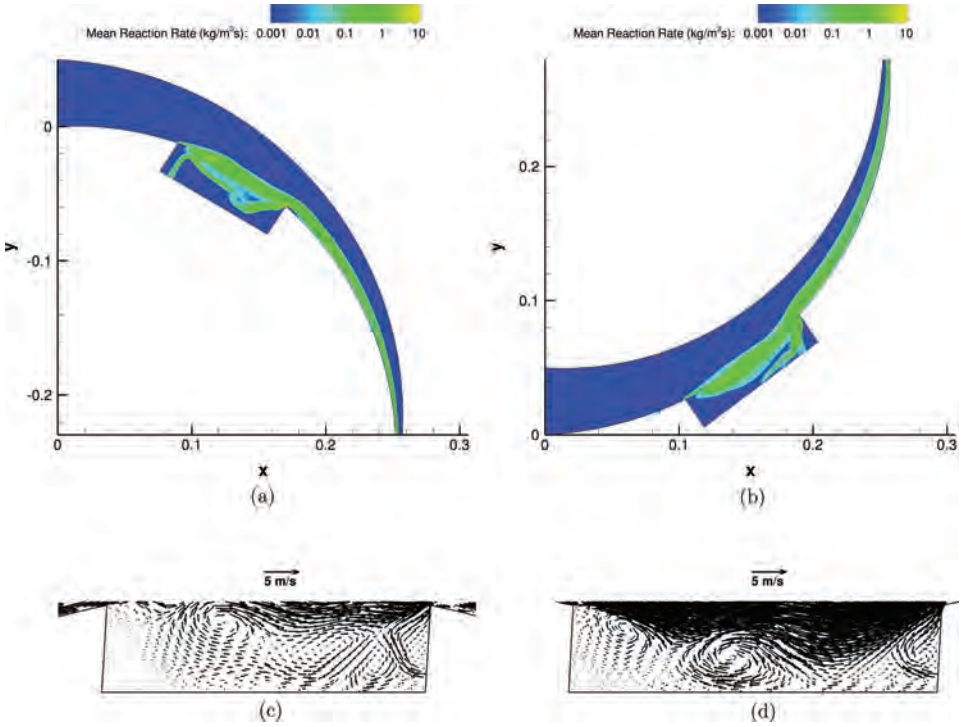

Figure 26: Time-averaged reaction rate and instantaneous velocity vectors in 2D, 90° turning, converging channels with 200×050 cavities at $Re = 2000$ with reinforcing injection.

Table 1: Summary of combustion efficiencies at $Re = 2000$

Cavity	100×050	200×050	200×050
Re	2000	2000	5000
Disrupting	0.716	0.758	0.915
Reinforcing	0.771	0.781	0.463
Parallel	0.760	0.754	0.508
Opposing	0.808	0.771	0.869

Table 2: Summary of 2D combustion efficiencies for low Mach number cases

Configuration				Injection scheme			
Cavity size	*Re*	Curvature	Convergence	Disrupting	Reinforcing	Opposing	Parallel
200 × 050	2000	–	–	0.758	0.781	0.771	0.754
200 × 050	2000	60° inside	–	0.736	0.746	0.757	0.741
200 × 050	2000	60° outside	–	0.756	0.781	0.797	0.767
200 × 050	2000	90° inside	–	0.715	0.732	0.730	0.737
200 × 050	2000	90° outside	–	0.814	0.800	0.821	0.791
200 × 050	2000	–	2:1	0.931	0.759	–	–
200 × 050	2000	–	4:1	0.957	0.954	–	–
200 × 050	2000	–	10:1	0.984	0.955	–	–
200 × 050	2000	90° inside	10:1	0.946	0.935	–	–
200 × 050	2000	90° outside	10:1	0.869	0.811	–	–
100 × 050	2000	–	–	0.716	0.771	0.812	0.760
200 × 050	5000	–	–	0.915	0.463	0.869	0.508

Table 3: Comparison of combustion efficiencies for high Mach number cases

Configuration				Inlet Mach number	
Cavity size	*Re*	Curvature	Convergence	0.0082	0.041
200 × 050	2000	–	10:1	0.984	0.899
200 × 050	2000	90° inside	10:1	0.946	0.914
200 × 050	2000	90° outside	10:1	0.869	0.819